49th AIAA Aerospace Sciences Meeting including the New Horizons Forum and Aerospace Exposition
4 - 7 January 2011, Orlando, Florida

AIAA 2011-544

Wind Turbine Performance Analysis Under Uncertainty

Giovanni Petrone* and Carlo de Nicola †
University of Naples "Federico II", Napoli, 80120, Italy

Domenico Quagliarella‡
Centro Italiano Ricerche Aerospaziali (CIRA), Capua, 81043, Italy

Jeroen Witteveen § and Gianluca Iaccarino¶
Mechanical Engineering Departement, Stanford University, Stanford, CA, 94305, USA.

The performance of wind turbines can be negatively affected by the presence of uncertainties. We introduce a comprehensive multi-physics computational model EOLO that enables the estimation of aerodynamic and structural characteristics assiociated with horizontal axis wind turbines, and use it to study the impact of uncertainties on the aerodynamic performance and noise. We consider variability in the wind conditions, manufacturing tolerances and roughness induced by insect contamination as sources of uncertainties and treat them within a probabilistic framework using Latin Hypercube Sampling and Stochastic Simplex Colocation. The results demonstrate that these two methods lead to a statistical characterization of the quantity of interest which is considerably faster than classical Monte Carlo methods. In addition, we demonstrate how the uncertainties impact the aerodynamics and noise leading to a largely inferior performance compared to the nominal design.

I. Introduction and motivations

Wind turbine reliability plays a critical role in the long-term evolution of wind-based energy generation. The computational assessment of failure probability or life expectancy of turbine components is fundamentally hindered by the presence of large uncertainties in both the environmental conditions and blade geometry and structure. Rigorous quantification of the impact of such uncertainties can fundamentally improve the state-of-the-art in computational predictions and, as a result, provide aid in the design of more cost-effective devices.

In the following we will describe a computational framework constructed around tools developed mainly at the National Renewable Energy Laboratory (NREL). These tools are essentially *deterministic*: once the wind-turbine configuration and other input conditions are specified, the solution is uniquely determined without vagueness. On the other hand, when uncertainties are present, the results have to be expressed in a non-deterministic fashion either probabilistically or as ranges of possible outcomes. In this work we focus on the former, and describe the uncertainties as random variables. At this point the computations become *probabilistic* in nature and it is necessary to propagate the input variability into the output of interest (quantity of interest, QoI). The approach we follow here is strictly non-intrusive, in the sense that the existing tools are used without modifications, but the solution - or more precisely, their probability distributions - are constructed performing an ensemble of deterministic analysis. One of the objectives of the present work is to compare two methodologies that aim at characterizing statistically the QoIs using a low number of deterministic solutions compared to classical Monte Carlo schemes. The two approaches are the Latin Hypercube Sampling (LHS) and the Stochastic Simplex Collocation (SSC) and are briefly described

*PhD. Student, Department of Aerospace Engineering, P.le Tecchio 80, 80120 Napoli, Italy.
†Professor, Department of Aerospace Engineering, P.le Tecchio 80, 80120 Napoli, Italy.
‡Senior Researcher, Department of Applied Aerodynamic and Aeroacoustics, Via Maiorise, 81043 Capua, Italy.
§Postdoctoral Fellow, Center for Turbulence Research, Stanford, CA, 94305, USA.
¶Assistant Professor, Mechanical Engineering Department, Stanford, CA, 94305, USA.

in Section III. The computational framework which has been developed and exercised in the present work is illustrated in Section II.

It is important to note that the first step in any uncertainty quantification procedure is the identification of the sources of uncertainties. We focus on wind conditions, blade manufacturing tolerances and insect contamination. In Section IV we gather information from literature regarding each one of these sources and perform analysis to assess their impact on both aerodynamic performance and noise.

II. EOLO: a multi-physics low-order model for wind turbines

Wind turbines are multi-physics devices in which the aerodynamic performance, the structural integrity of the blades, the energy conversion toolbox and the acoustic impact have to be carefully examined to achieve an effective design. Each one of these aspects introduces considerable hurdles for detailed simulations. The aerodynamic performance is dominated by the design of the blade cross-sections. The sections are typically laminar-flow airfoils to reduce the overall drag. The flow characterization is complicated by the need to predict laminar/turbulent transition under a variety of clean and perturbed wind conditions, the inherent angle of attack variability associated to rotation, the presence of dynamic stall, aeroelasticity, etc. In spite of the development of advanced computational fluid dynamic tools that can predict with reasonable accuracy the aerodynamic performance of rotors,[1] the computations remain extremely expensive and often rely on simple models to capture important effects, such as transition, and are generally not considered to be predictive for extreme events such as stall. In this work, we focus on building a flexible computational infrastructure based on low-fidelity models that are connected together in a *matlab* environment called `EOLO`. There are two main advantages resulting from this choice: *i)* control and flexibility in using different models developed for capturing complex phenomena, *ii)* low computational cost. It is the second aspect that fundamentally enables us to perform analysis under uncertainty.

In the following we introduce the various computational tools that are used to perform the deterministic analysis. The uncertainty quantification methodologies are described in the next section.

II.A. Aerodynamic analysis

The geometrical description of the turbine blades is based on the specification of three airfoils at the root, mid-span and tip. Simple linear interpolation is used to construct the geometry at the other cross-sections and the local aerodynamic (e.g. two-dimensional) analysis is carried out using a potential flow method with interactive viscous correction. The tool we used is `Xfoil`[9] which includes a model for boundary layer transition based on the e^N method. `Xfoil` is used to determine the aerodynamic force coefficients polars in a range of angle of attacks from $-15°$ to $25°$ to cover the range of incident angles experienced during a full rotation. `Xfoil` is not expected to be accurate in the prediction of stall, because of the presence of extensive flow separation and possibly unsteady effects.

Hence a correction to the polar curve is introduced, based on Viterna[10] and Corrigan models which provide a correction of the lift and drag coefficient at high angle of attack. A final correction to the aerodynamic coefficients is employed due to the presence of finite-span effects. Here we use a modification based on the Lanchester- Prandtl theory

$$C_L = C_L^{'}; \quad C_D = C_D^{'} + \frac{Cl^2}{\pi AR}; \quad \alpha = \alpha^{'} + \frac{Cl}{\pi AR} \tag{1}$$

where C_L and $C_L^{'}$, C_D and $C_D^{'}$, α and $\alpha^{'}$ are the finite and infinite span airfoil lift coefficients, drag coefficients and angles of attack respectively and AR is the aspect ratio of the wind blade.

The Viterna model estimates the lift and drag coefficients (when $\alpha > \alpha_s$) as follows

$$C_L = \frac{C_{Dmax}}{2}\sin 2\alpha + K_L\frac{\cos\alpha^2}{\sin\alpha}; \quad C_D = C_{Dmax}\sin\alpha^2 + K_D\cos\alpha \tag{2}$$

$$K_L = (C_{LS} - C_{Dmax}\sin\alpha_s\cos\alpha_s)\frac{\sin\alpha_s}{\cos\alpha_s^2}; \quad K_D = \frac{C_{DS} - C_{Dmax}\sin\alpha_s^2}{\cos\alpha_s} \tag{3}$$

where α_s is the finite span airfoil stall angle, C_{LS} and C_{DS} are the finite span airfoil lift and drag coefficient

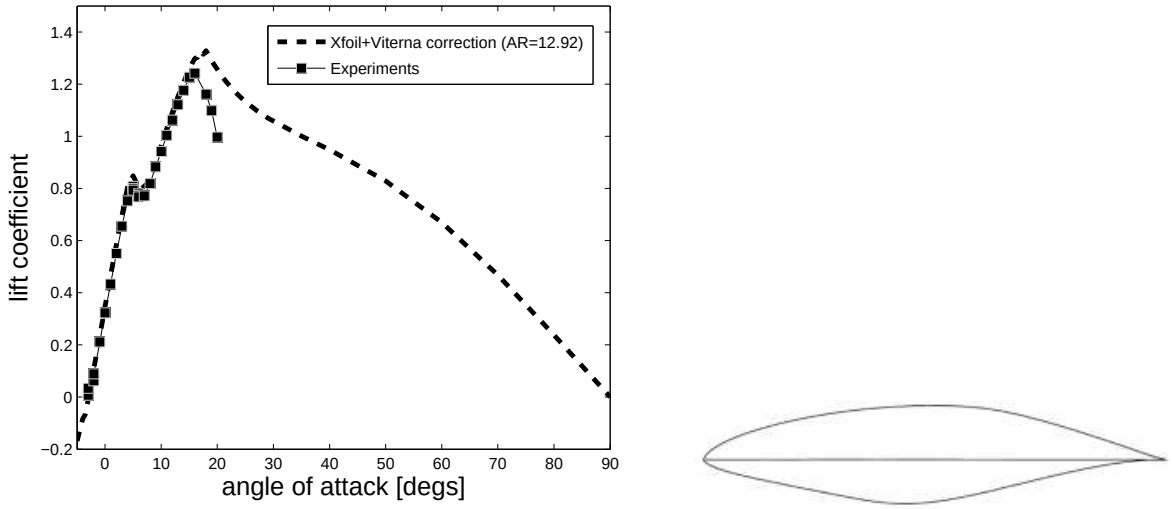

Figure 1. NREL s827 airfoil (right); predictions of the lift coefficient (left) at M=0.1, Re=3e6 under natural transition conditions.

at stall angle and C_{Dmax} is the finite span airfoil maximum drag coefficient

$$\begin{aligned} C_{Dmax} &= 1.11 + 0.018AR \quad AR \leq 50 \\ C_{Dmax} &= 2.01 \qquad\qquad\quad AR > 50 \end{aligned} \tag{4}$$

The models described above are included in a tool called `Viterna` which collects the polars from `Xfoil` and introduces stall and finite-span corrections. The present predictions of the lift curve are reported for the NREL S827 airfoil in Fig.1.

II.B. Structural analysis

Fluid structure interactions play an important role in the determination of the structural integrity of the turbine blades and in the overall aerodynamic performance.

The geometrical description of the blade is used as a starting point to define span-varying properties relevant to its composite structure. The NREL `PreComp`[2] computes cross-coupled stiffness, inertia and offsets of the blade shear center, tension center, and center of mass with respect to the blade pitch axis. These quantities are then used to determine a low-order model for the rotor, tower and drivetrain shaft. Specifically, the characteristics of a rotating-beam equivalent to the blade are computed using NREL `BModes`,[5] a finite-element code that evaluates the deformation modes.

II.C. Performance analysis

The `Viterna` corrected polars at certain nodes along the span, the flapwise and edgewise `Bmodes` modal shapes and the `PreComp` properties are then used as input to NREL `FAST`[3] (Fatigue, Aerodynamics, Structures, and Turbulence) which is a comprehensive aeroelastic simulator capable of predicting both the extreme and fatigue loads of two- and three-bladed horizontal-axis wind turbines.

This code is based on the NREL `AeroDyn`[4] solver, an element-level wind-turbine aerodynamic analysis routine. It requires information on the status of a wind turbine from the dynamics analysis routine and a *wind file* describing the atmospheric conditions. It returns the aerodynamic loads for each blade element to the dynamics routines.

II.D. Wind conditions

The aerodynamic performance of wind turbines is dominated by the wind conditions. Atmospheric boundary layers are subject to large variability in wind direction and intensity with largely unsteady dynamics and frequent gusts. In `EOLO` we generate realistic wind conditions using the NREL `TurbSim`[6] tool, which constructs a stochastic inflow with a precisely specific velocity fluctuation spectrum.

II.E. Acoustic analysis

The NREL prediction of aeroacoustic noise is based on six different noise sources (Fig. 2) that are assumed to independently generate their own noise signature. The assumption of independence is based on the idea that the mechanisms for each noise source(namely turbulent boundary layer trailing edge, separating flow, laminar boundary layer vortex shedding, trailing edge bluntness vortex shedding, and tip vortex formation[24,26]) are fundamentally different from each other or occur in different locations along a turbine blade, such that they do not interfere with one another.

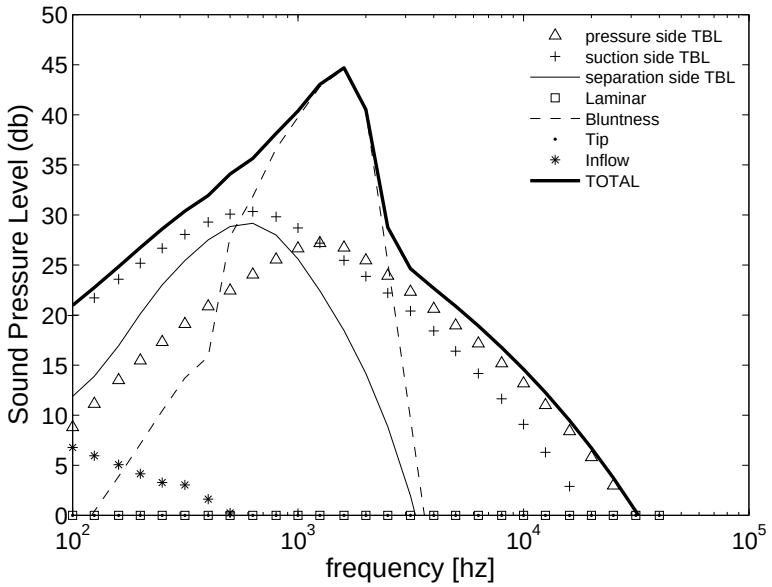

Figure 2. Breakdown of the noise generated by a 50kw wind turbine at a microphone located at (x,y,z)=(-20m,0m,0m)

II.F. the `EOLO` matlab script

The various tools briefly described in the previous subsections are glued together in a multi-physics simulation process using `matlab`. The overall driver script, `EOLO` handles the transfer of information between the various tools and then collects the final outputs and computes statistics. A flowchart of the process is reported in Fig. 3; it is clear that modifications to the framework can be handled in a simple way, for example substituting the aerodynamic performance evaluation module (`Xfoil` and `Viterna`) with a computational fluid dynamic solver. `EOLO` also provides a unique interface for the entire process (from inputs to outputs) that is directly connected to the uncertainty quantification tools presented in the next section.

III. Uncertainty analysis

The simulation environment described above can be effectively used to study wind turbine performance in the absence of uncertainties. In this section we introduce two methodologies that enable us to characterize the effect of variability in wind conditions, manufacturing tolerance and insect contamination. As mentioned earlier we limit our analysis to uncertainties that can be described using random variables (aleatory uncertainties) and, therefore, our goal is to construct a probabilistic framework around the `EOLO` environment. The most straightforward choice is to perform Monte Carlo (MC) sampling in which many deterministic simulations corresponding to randomly chosen wind conditions for example, are performed and a statistical characterization is obtained directly from this ensemble. It is well known that typically a very large ensemble is required to achieve convergence of the QoI statistics. In the following, we introduce two alternative approaches that allow us to obtain equivalent results using very few `EOLO` simulations. In the following, we generally refer to the input uncertain variables as ξ and refer to the *space* spanned by these variables as the *parameter* (or probability) space to distinguish it from the space of the physical variables.

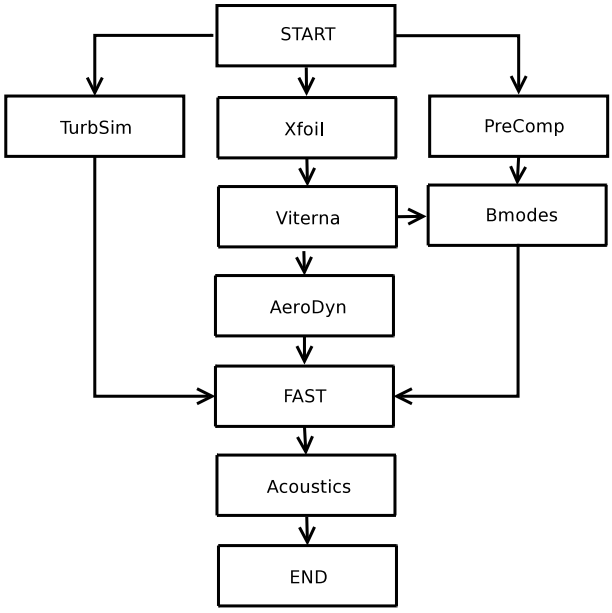

Figure 3. Multi-physics computational framework to perform analysis of wind turbine: EOLO flowchart

III.A. Latin Hypercube Sampling (LHS)

In Monte Carlo methods, a sequence $\xi_1, \xi_2, \ldots, \xi_n$ is sampled according to the probability distribution of ξ, which is assumed to be known. Simulations are performed for each sample ξ_i to obtain the QoIs and build an empirical density function that converges to the actual probability density function of the QoI as n increases.

Several methods have been developed to accelerate the MC approach. One of the most successful is the Latin Hypercube sampling (LHS) approach. LHS is a stratified-random procedure which provides an efficient way of sampling variables from their distributions.[31] The cumulative distribution for each input variable is divided into N equiprobable intervals. A value is selected randomly from each $i-th$ interval and the sampled cumulative probability can be written as:[32]

$$p_i = \frac{1}{N} r_u + (i-1)N \tag{5}$$

where r_u is a uniformly distributed random number ranging from 0 to 1. The N values obtained for each variable are paired randomly with the other variables to construct a sample point in the parameter space. Unlike simple random sampling, this method ensures full coverage of each variable range by optimally stratifying each marginal distribution.

III.B. Stochastic Simplex Collocation (SSC)

Due to the relatively slow convergence rate of Monte Carlo simulations, other uncertainty quantification methods have been developed based on a polynomial approximation of the response. Stochastic Collocation (SC) is a widely used example of such a method, which is based on sampling Gauss quadrature points and using Lagrangian polynomial interpolation in probability space. However, due to the structured grid of the quadrature points in multiple random dimensions, the spectral convergence of the Stochastic Collocation method reduces significantly with an increasing number of uncertainties.

Here, the Simplex Stochastic Collocation (SSC) method[7,8] is presented that combines the effectiveness of random sampling in higher dimensions with the accuracy of polynomial interpolation. It also leads to the superlinear convergence behavior of Stochastic Collocation methods and the robustness of Monte Carlo approaches. SSC discretizes the parameter space Ξ using non-overlapping simplex elements Ξ_j from a Delaunay triangulation of sampling points, with $\Xi = \bigcup_{j=1}^{n_e} \Xi_j$, where n_e is the number of elements. In each of the simplexes Ξ_j, the response surface of the quantity of interest, $u(\boldsymbol{\xi})$ as function of the random

parameters $\boldsymbol{\xi} \in \Xi$, is approximated by a polynomial $w_j(\boldsymbol{\xi})$

$$w_j(\boldsymbol{\xi}) = \sum_{m=0}^{P} c_{j,m} \Psi_{j,m}(\boldsymbol{\xi}), \tag{6}$$

with $P+1$ coefficients $c_{j,m}$ and basis polynomials $\Psi_{j,m}(\boldsymbol{\xi})$. The polynomials are found by interpolation of the samples $v_k = u(\boldsymbol{\xi}_k)$ at the vertexes $\boldsymbol{\xi}_k$ of the simplex elements, with $k = 1, \ldots, n_\mathrm{s}$, where n_s is the number of samples. For higher degree interpolation a stencil of sampling points $v_{k_{j,l}}$ at the vertexes $\xi_{k_{j,l}}$ of surrounding simplexes is constructed, with $l = 0, \ldots, N$ and $k_{j,l} \in \{1, \ldots, n_\mathrm{s}\}$. The polynomial coefficients $c_{j,m}$ are then given by

$$\begin{bmatrix} \Psi_{j,0}(\boldsymbol{\xi}_{k_{j,0}}) & \Psi_{j,1}(\boldsymbol{\xi}_{k_{j,0}}) & \cdots & \Psi_{j,P}(\boldsymbol{\xi}_{k_{j,0}}) \\ \Psi_{j,0}(\boldsymbol{\xi}_{k_{j,1}}) & \Psi_{j,1}(\boldsymbol{\xi}_{k_{j,1}}) & \cdots & \Psi_{j,P}(\boldsymbol{\xi}_{k_{j,1}}) \\ \vdots & \vdots & \ddots & \vdots \\ \Psi_{j,0}(\boldsymbol{\xi}_{k_{j,N}}) & \Psi_{j,1}(\boldsymbol{\xi}_{k_{j,N}}) & \cdots & \Psi_{j,P}(\boldsymbol{\xi}_{k_{j,N}}) \end{bmatrix} \begin{pmatrix} c_{j,0} \\ c_{j,1} \\ \vdots \\ c_{j,P} \end{pmatrix} = \begin{pmatrix} v_{k_{j,0}} \\ v_{k_{j,1}} \\ \vdots \\ v_{k_{j,N}} \end{pmatrix}, \tag{7}$$

with $\mathrm{N} \geq \mathrm{P}$. The robustness of the approximation is guaranteed by using a limiter approach for the local polynomial degree p_j, based on the extension of the Local Extremum Diminishing (LED) concept to probability space. This ensures that no overshoots are present in the response interpolation in each of the elements Ξ_j

$$\min_{\Xi_j}(w_j(\boldsymbol{\xi})) \geq \min_{\Xi_j}(u(\boldsymbol{\xi})) \ \wedge \ \max_{\Xi_J}(w_j(\boldsymbol{\xi})) \leq \max_{\Xi_j}(u(\boldsymbol{\xi})), \tag{8}$$

for $j = 1, \ldots, n_\mathrm{e}$. The initial samples are located at the parameter range extrema and one at the nominal conditions, see Figure 4a for a two-dimensional example. The discretization is adaptively refined by calculating a refinement measure based on a local error estimate in each of the simplex elements. A new sampling point is then added randomly in the simplex with the highest measure and the Delaunay triangulation is updated. The sample is confined to a sub-domain of the simplex to ensure a good spread of the sampling points, see Figure 4a. The refinement to $n_\mathrm{s} = 17$ samples, shown in Figure 4, leads to a super-linear convergence by increasing the polynomial degree p_j with the increasing number of available samples n_s. The sampling procedure is stopped when a global error estimate reaches an accuracy threshold.

(a) Refinement of the initial mesh

(b) Refined mesh for 17 samples

Figure 4. Simplex Stochastic Collocation discretization of a two–dimensional probability space.

In the wind turbine simulations and other large-scale problems, it is possible that one of the deterministic computations for a specific sample of the random parameters does not converge or gives an unrealistic result. For the Stochastic Collocation method such a failure of one of the quadrature samples would be a serious problem in computing statistical moments. On the other hand, this situation forms no obstacle for SSC owing to the flexibility of the randomized sampling. It is handled by introducing a check of the correct execution of the samples into the algorithm. If an unconverged sample is detected, then the failed sample computation is automatically restarted for another randomly sampled point in the refined simplex element. In the analysis performed in this paper, this has proven to be an effective approach for dealing with erroneous samples, which shows the flexibility of the SSC method in complex computational problems.

IV. Data assimilation

IV.A. Uncertain meteorological conditions

The energy produced by a wind turbine is usually expressed as an annual average. Since production falls off dramatically as the wind speed drops, most of the time the wind turbine is producing well below its expected rate.[16] It is important to characterize the wind turbine behavior resulting from the measured wind variability to assess the effective performance.

For land based turbines, the wind speed distribution is usually approximated by a Weibull fit.[11] As an example, Downey[15] extracted data from the database http://winddata.com of eight sites that have wind speed measurements above 60 m in height.

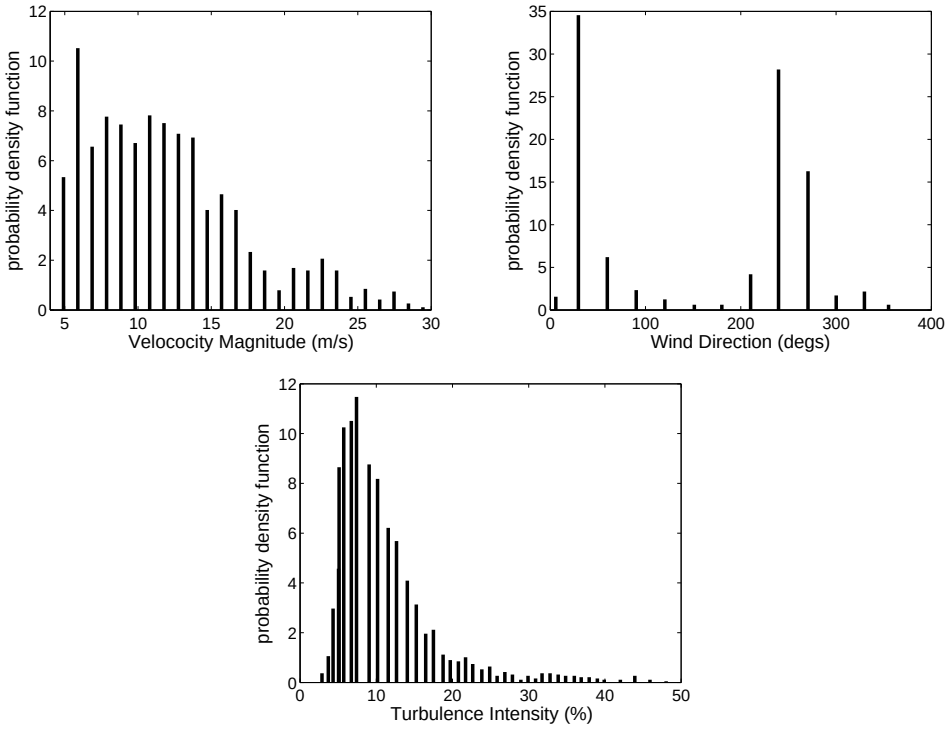

Figure 5. Wind speed, direction and turbulence intensity at the Acqua Spruzza, Italy site. The data is reported in terms of empirical probability distributions scaled from 40 to 24 meters.

Following the same approach we extracted nominal wind speed, turbulence intensity and direction data at a site (Acqua Spruzza, Italy) where a wind turbine farm was built by ENEL S.p.A. to evaluate the performance of commercial medium-sized turbines operating in complex terrain and very hostile climate. A large collection of wind measurements is summarized in Fig. 5 in terms of wind speed and direction and turbulence intensity. The histograms of these three random variables are used directly as input for the uncertainty propagation methods described previously, after being converted into continuous probability density functions (for each of the input variables) via linear interpolation. Note that no information regarding the correlation of the three random variables is available, and therefore we assume that the inputs are independent.

The wind data readily available provide an estimate of the wind speed at a certain height. To construct the wind conditions at the actual rotor hub height (≈ 24 meters) we use a classical[13] scaling law:

$$\frac{U(z_2)}{U(z_1)} = \frac{ln(z_2/z_0) - \Psi(Z_2/L)}{ln(z_1/z_0) - \Psi(Z_1/L)} \tag{9}$$

where L is the Monin-Obukhov length [m], U is the wind speed [m/s], z is the height [m], z_0 is the terrain roughness [m] and Ψ is the stability function.[16] Eq. (9) uses a logarithmic velocity profile dependent on terrain roughness z_0 plus an atmospheric stability correction Ψ dependent on the ratio of height, z, and Monin Obukhov length, L. Turbulence may be produced by shear (speed differences) or by buoyancy (density

differences); the length L is the height at which shear and buoyancy produce the same amount of turbulent kinetic energy. The Monin-Obukhov length L must be estimated. When the wind speed is sufficiently high (above $6m/s$) thermal effects play no role above land, and neutrality may be assumed,[14] $\Psi = 0$. In this case the wind speed follows a logarithmic profile determined by terrain roughness z_0 and Eq. (9) reduces to

$$\frac{U(z_2)}{U(z_1)} = \frac{ln(z_2/z_0)}{ln(z_1/z_0)} \tag{10}$$

The roughness of the terrain z_0 may be estimated with the Petersen classification[12] or from measurements of turbulence intensity I at some reference height z_r , using:

$$z_0 = z_r exp(\frac{-1}{I(z_r)}) \tag{11}$$

IV.B. Insect contamination

Several studies on wind turbines[17–20] and fixed wings[21,22] illustrate the effect of insect and dirt contamination on the overall aerodynamic performance. Insects are present in the lower layer of the atmosphere, with a density rapidly decreasing from ground level to 500 ft. Hardy and Milnecite[23] found that the morphology of insects is a function of the altitude and that estimation of the actual contamination depends on the operating conditions. In wind-turbines the effect of contamination can be particularly strong when the blade cross-sections are designed to support mostly laminar flows. The presence of insect contamination produces boundary layer disturbances that can lead to early transition to turbulence with a deterioration of the aerodynamic performance. This is the motivation for including insect contamination as a leading cause of uncertainty in the analysis of wind turbines.

Crouch *et al*[25] studied experimentally the effects of surface protrusions (steps) on the transition to turbulence in boundary layers. They also modified the e^N method to capture the observed transition modifications, via a reduction of the critical N-factor:

$$N_{crit} = N_{crit^0} - \Delta N_{crit}(\frac{h}{\delta^*}) \tag{12}$$

where h is the height of the step (i.e. the accumulated insect height)[m], δ^* is the boundary layer displacement thickness at the step location [m], ΔN_{crit} accounts for the local change in the stability characteristics at the step[-] and N_{crit^0} is the clean value of the critical n-factor[-].

In this work we assume that the insect impact produces a roughness that leads to a possible modification of the N-factor. We consider three independent variables describing the N-factor ranging from clean conditions ($N_{crit} = 9$) to transition bypass ($N_{crit} = 1$) at the root, midspan and tip sections.

IV.C. Manufacturing tolerances

There is a general agreement that airfoil shape, twist and chord length imperfections are detrimental to aerodynamic performance, but only limited quantitative data is available in the open literature about their origin and quantitative effects. Loeven and Bijl[30] used a Polynomial Chaos Framework for the quantification of airfoil geometrical uncertainties. Ilinca, Hay, and Pelletier[27] treat shape sensitivities of unsteady laminar flow around a cylinder in ground proximity. Etienne*et al*[28] investigated shape sensitivities of flexible plates in a flow domain. Gumber, Newman, and Hou[29] included first order moments in robust design optimization of a 3D flexible wing with uncertain wing geometry. The geometry of a manufactured wind turbine airfoil is generally different from the nominal design mainly because of manufacturing tolerances. It is generally difficult to characterize probabilistically the effect of these tolerances; in this work we focus on errors associated with the protusion process, where the blade is constructed as a sequence of cross-section. We assume that the twist of the blade (the section orientation with respect to a nominal plane) is imprecise. As before, we assume that we can describe the uncertainty using three independent parameters (with uniform probability distributions ranging from -2° to 2°) associated to the twist at the root, the midspan and the tip section.

V. Analysis under uncertainty

The AOC 15/50 is a downwind turbine, i.e. its blades rotate downwind of the drive train assembly. Furthermore, it has no active yaw control and depends on its blades to track the wind. This wind turbine is

the evolution of the rugged and reliable Enertech E44, many of which were installed in the 1980's and are still running today. Independent analysis and testing at NREL, the Netherlands Energy Research Foundation (ECN), RISO Laboratory in Denmark, the Atlantic Wind Test Site (AWTS) on Prince Edward Island and other sites around the world verify that the AOC 15/50 wind turbine generators are very reliable in even the harshest weather conditions. The AOC 15/50 is designed for simplicity to minimize maintenance requirements and to be able to safely operate in normal and extreme conditions. The principal characteristics of the AOC 15/50 can be found in Table 1.

Table 1. AOC 15/50 wind turbine, principal characteristics

Type	Grid Connected
Configuration	Horizontal Axis
Axis Rotor Diameter	15 m
Centerline Hub Height	25 m
Rated Electrical Power	50 kW @ 11.3 m/s
Cut in [-]	4.6 m/s
Shut down (high wind)	22.4 m/s
Type of Hub	Fixed Pitch Rotor
Diameter	15 m
Swept Area	177 m^2
Number of Blades	3
Rotor Solidity	0.077
Rotor Speed @ rated wind speed	65 rpm
Location Relative to Tower	Downwind
Cone Angle	6^o
Tilt Angle	0^o
Rotor Tip Speed	51 m/s @ 60 Hz
Design Tip Speed	6.1
Length	7.2 m
Material	Epoxy /glass fibre
Airfoil (type)	NREL, Thick Series, modified
Twist	7^o
Blade Weight	150 kg approximate
Yaw	Free, rotates 360 degrees

V.A. Uncertain meteorological conditions

In this section the AOC 15/50 has been investigated using the uncertain meteorological conditions of Figure 5. In this case `EOLO` is driven by the SSC routines and the uncertainties are injected trough Turbsim; the statistics are constructed performing an ensemble of deterministic analysis. For reasons of economy, the wind history during the turbine's approximately twenty year life is reduced to 10 minute periods (or load cases) at each wind speed.[16] The latitude chosen for the turbulence model is 41 degrees, matching the data extracted from the Acqua Spruzza site. The Von Karman spectral model for the meteorological boundary conditions has been chosen in this application, assuming neutral atmospheric condition.[33,34] The AOC 15/50 deterministic conditions chosen as reference in this work are illustrated in Table 2.

The Monte Carlo samples on the response surface obtained by the simplex reconstruction are shown in Figure 6; the reader can notice that the samples follow the input distribution of Figure 5.

A three color (red to blue) map has been introduced to relate the samples to the effective value of the power coefficient in the domain: the red points correspond to high power extracted by the wind turbine. The

Table 2. AOC 15/50 wind turbine, deterministic conditions

Wind speed	6 m/s
Turbulence intensity	5%
Wind direction	0^o
Latitude	41^o
Working time	10 min
Rotor speed	55 rpm

map reveals that improved efficiency is achieved for moderate wind speeds (5-12 m/s) and low turbulence levels (2-10 percent), while other conditions lead to decreased performance.

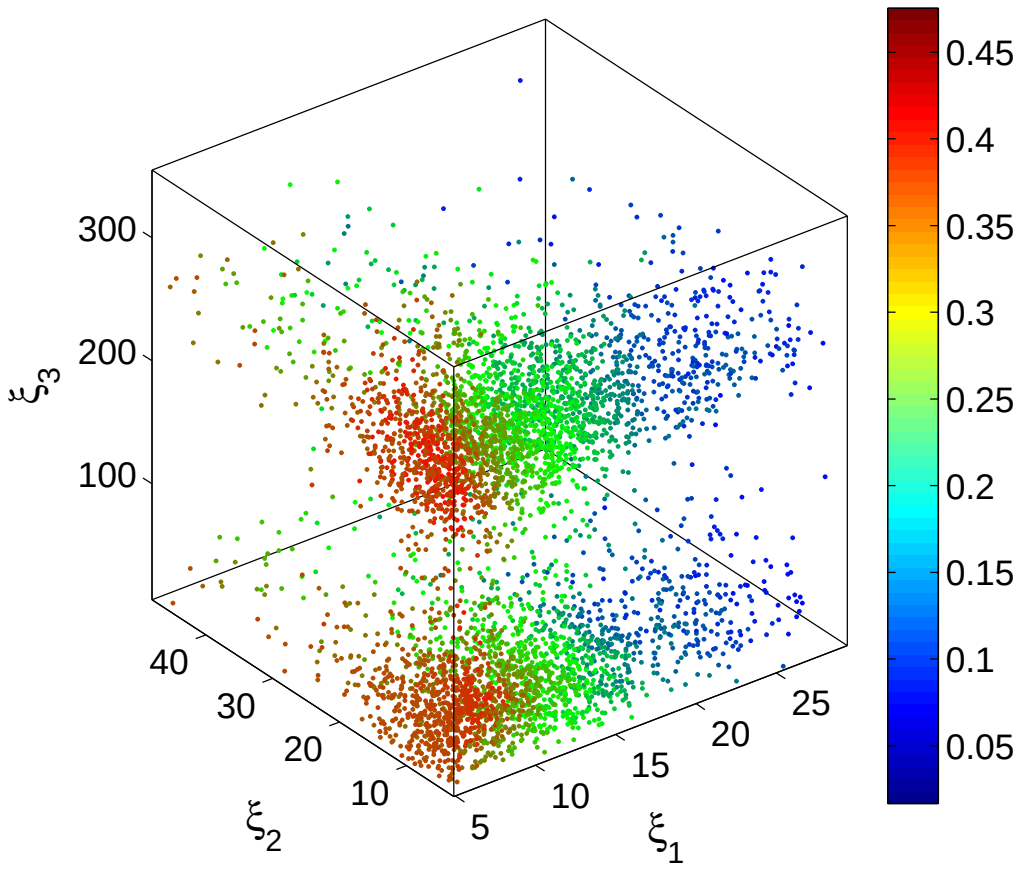

Figure 6. Monte Carlo samples for meteorological conditions.

Since the cut-off speed of the AOC 15/50 is 22.4 m/s, placing the wind turbine in the site of interest would likely lead to off-design operating conditions: the average power coefficient drops from 0.4596 to 0.2776.

The resulting cumulative probability distribution functions (CDF) for the power coefficient and the sound pressure level as a result of the varying meteorological conditions are shown in Figure 7. The output CDFs show approximately uniform distributions, in contrast with the input density for the meteorological conditions of Figure 5. The probability distributions fall completely below the deterministic characteristics of the wind turbine (Table 2) given by the vertical lines. The uncertain output for the power coefficient ranges from approximately 0 to the deterministic value of approximately 0.45. The sound pressure level varies uniformly between 34 to 45 dB. These results show that the realistic uncertainty in the wind speed,

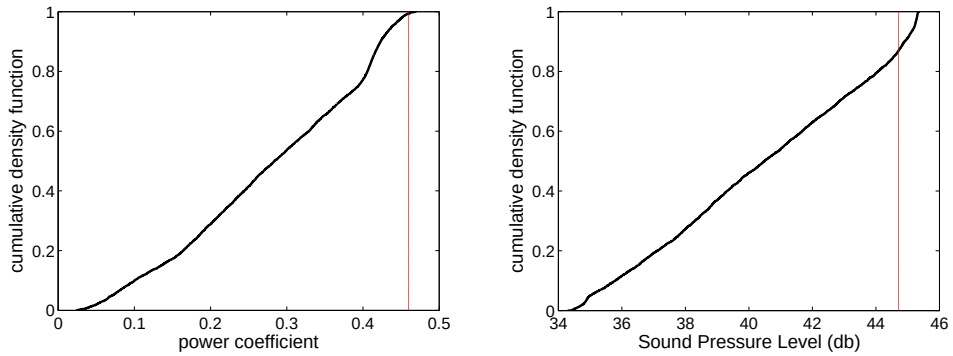

Figure 7. Meteorological conditions: cumulative density function of the power coefficient and Sound Pressure Level. The red lines represent the deterministic conditions.

direction, and turbulence intensity has a large impact on the wind turbine performance.

The convergence of the mean and standard deviation of the power coefficient and sound pressure level is shown in Figures 8 and 9 up to 70 samples in the SSC discretization. The mean values of the two outputs show fast convergence in the first 20 samples to a value significantly lower than the deterministic value. Increasing the number of deterministic solves to 70 does not significantly change the mean value. This is confirmed by the decreasing error estimate intervals with an increasing number of samples. The higher moment of the standard deviation shows, as expected, a slower convergence up to 40 samples with a relatively larger error estimate margin.

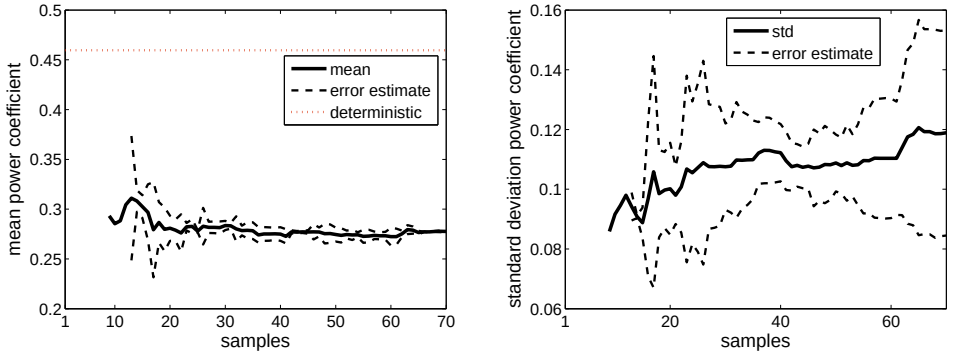

Figure 8. Meteorological conditions: convergence histories of the mean,variance and error of the power coefficient

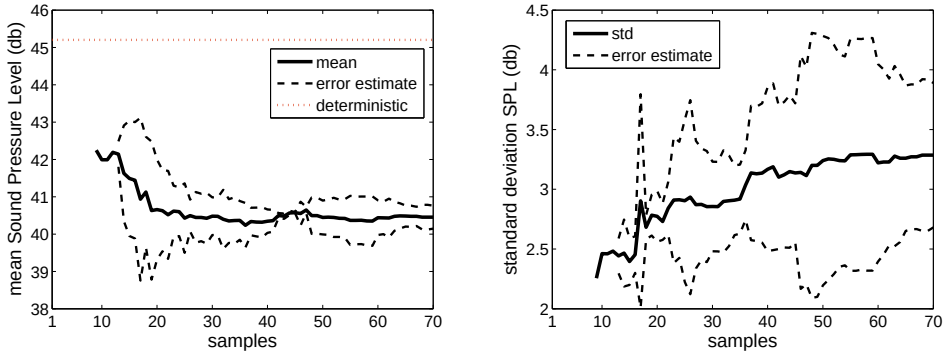

Figure 9. Meteorological conditions: convergence histories of the mean,variance and error of the Sound Pressure Level

The values for the mean and standard deviation at 70 samples are also compared to the nominal clean configuration in Table 3. Due to the uncertainty the mean power output almost halves, while the sound level is only moderately lower than the deterministic values. This demonstrates that the uncertain meteorological

conditions result in a significant reduction of the power performance of the wind turbine, which shows the need to optimize the wind turbine design under uncertain operating conditions. The relatively large coefficients of variation in the power coefficient and the sound pressure level up to 42.8% and 8.1%, respectively, are also reported.

Table 3. Analysis under uncertain meteorological conditions

Objective	Mean	Standard deviation	Coefficient of variation	Clean configuration
# Power Coefficient [-]	0.2776	0.1189	0.4283	0.4596
# Sound Pressure Level [*db*]	40.4530	3.2853	0.0812	44.711

V.B. SSC and LHS: a comparison

The convergence histories for the mean and standard deviation of the power coefficient and sound level are more closely examined in Figures 10 and 11.

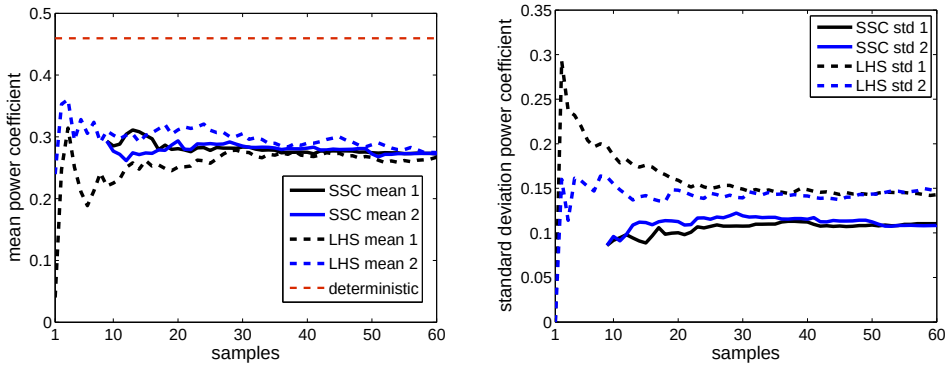

Figure 10. Meteorological conditions: comparison of the mean and variance of the power coefficient for two different SSC and two different LHS

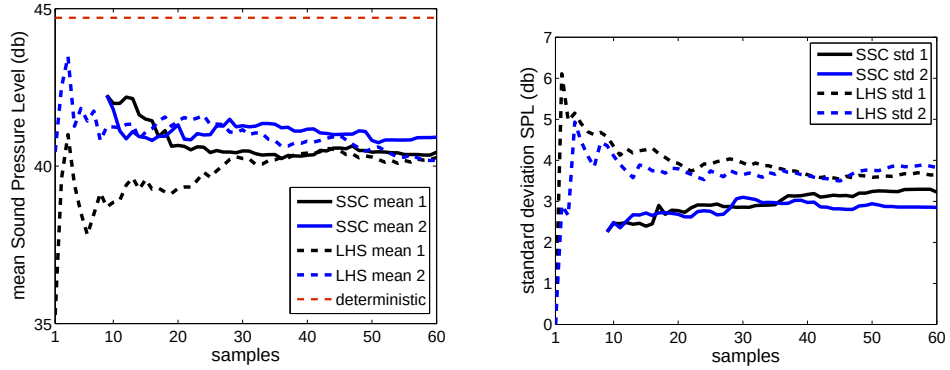

Figure 11. Meteorological conditions: comparison of the mean and variance of the Sound Pressure Level for two different SSC and two different LHS

The results of SSC and LHS are shown for two independent ensembles to illustrate the relative sensitivity as both methods rely on random sampling. This is clearly visible in the LHS results for the power in Figure 10 given a small number of samples (up to 40). For a larger sample size the two LHS results show improved agreement. The variations in the SSC results for the power coefficient are smaller than for LHS.

For the mean power output, the two methods show good agreement. The prediction of the standard deviation by LHS and SSC show a slightly different value, because we hypothesize that more than 60 samples are required to obtain convergence. The results for the sound level in Figure 11 show a relatively larger variation between the SSC runs and also gives a larger standard deviation output for LHS than for SSC.

V.C. Insect contamination

In this section the AOC 15/50 is investigated using the uniform distributions of section IV.B. In this case `EOLO` is driven by the SSC routines and the uncertainties are injected through the aerodynamic coefficients computed in `Xfoil`.

The Monte Carlo samples on the response surface obtained by the simplex reconstruction are shown in Figure 12; the spread of the samples follows the uniform input distribution.

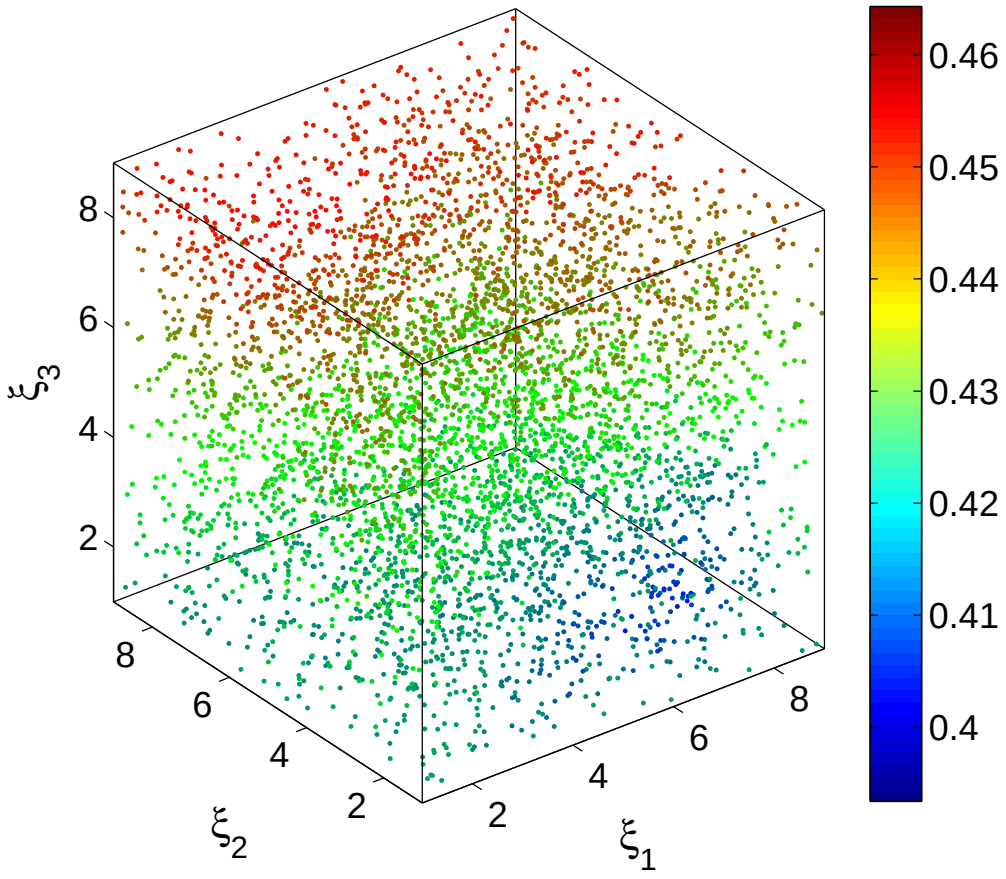

Figure 12. Monte Carlo samples for insect contamination

The colormap reveals that higher values of the n-critical factor (e.g. lower contamination) at tip region, ξ_3 primarly, as well as at mid-span region,ξ_2, lead to better performance: this can be justified due to the highest contribution of the outer airfoils to the mechanical torque at the shaft.

This analysis illustrates a reduction of up to 16% in the power coefficient (Figure 13) due to the insect contamination, while in the literature an effect of up to 50% has been reported.[17,18] This difference might be due to the present approach used to characterize the effect of the insect contamination. The variation of the perceived level of noise due to this source of uncertainty can be neglected.

Figure 15 and Figure 16 show the SSC convergence of the mean and the standard deviation of the output of interest. The error estimate is lower under uncertain meteorological conditions, therefore a smaller number of simplex points could have been used.

The mean, standard deviation and coefficient of variation of the analysis under insect contamination are summarized in Table 4.

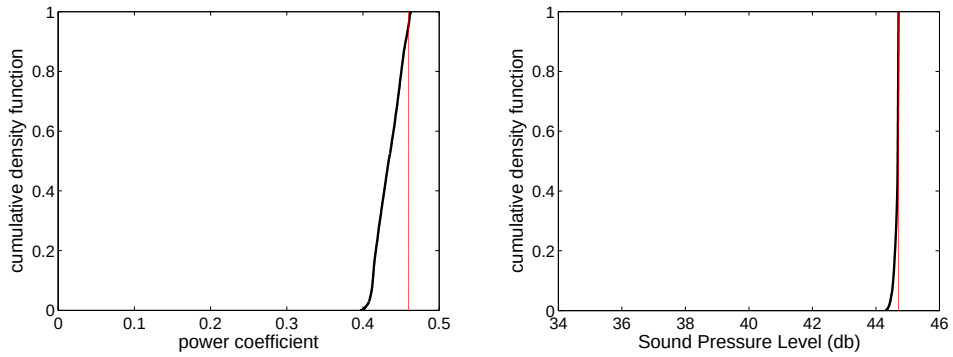

Figure 13. Insect contamination: cumulative density function of the power coefficient and Sound Pressure Level

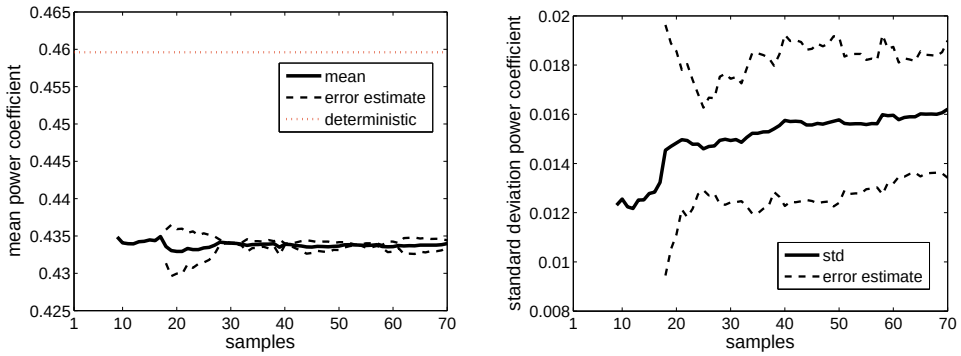

Figure 14. Insect contamination: convergence histories of the mean,variance and error of the power coefficient

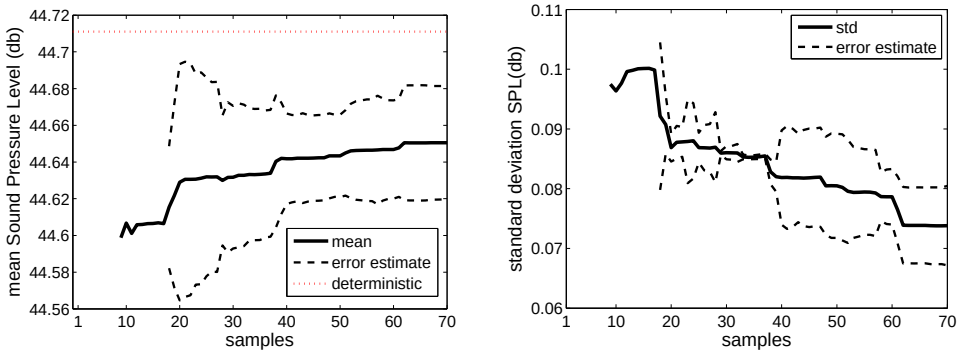

Figure 15. Insect contamination: convergence histories of the mean,variance and error of the Sound Pressure Level

Table 4. Analysis under insect contamination

Objective	Mean	Standard deviation	Coefficient of variation	Clean configuration
# Power Coefficient[-]	0.4340	0.0162	0.0373	0.4596
# Sound Pressure Level[*db*]	44.6505	0.0738	0.0017	44.711

V.D. Manufacturing errors

In this section the AOC 15/50 is investigated using the uniform distributions of section IV.C. In this case `EOLO` is driven by the SSC routines and the uncertainties are injected through the geometry pre-processor. The Monte Carlo samples on the response surface obtained by the simplex reconstruction are shown in Figure 12;

similar to the insect contamination case, the samples have a uniform distribution in the probability space. The colormap reveals that decreasing the twist in the mid-span region, ξ_2, leads to better performance: this can justify a novel robust shape optimization involving the twist distribution.

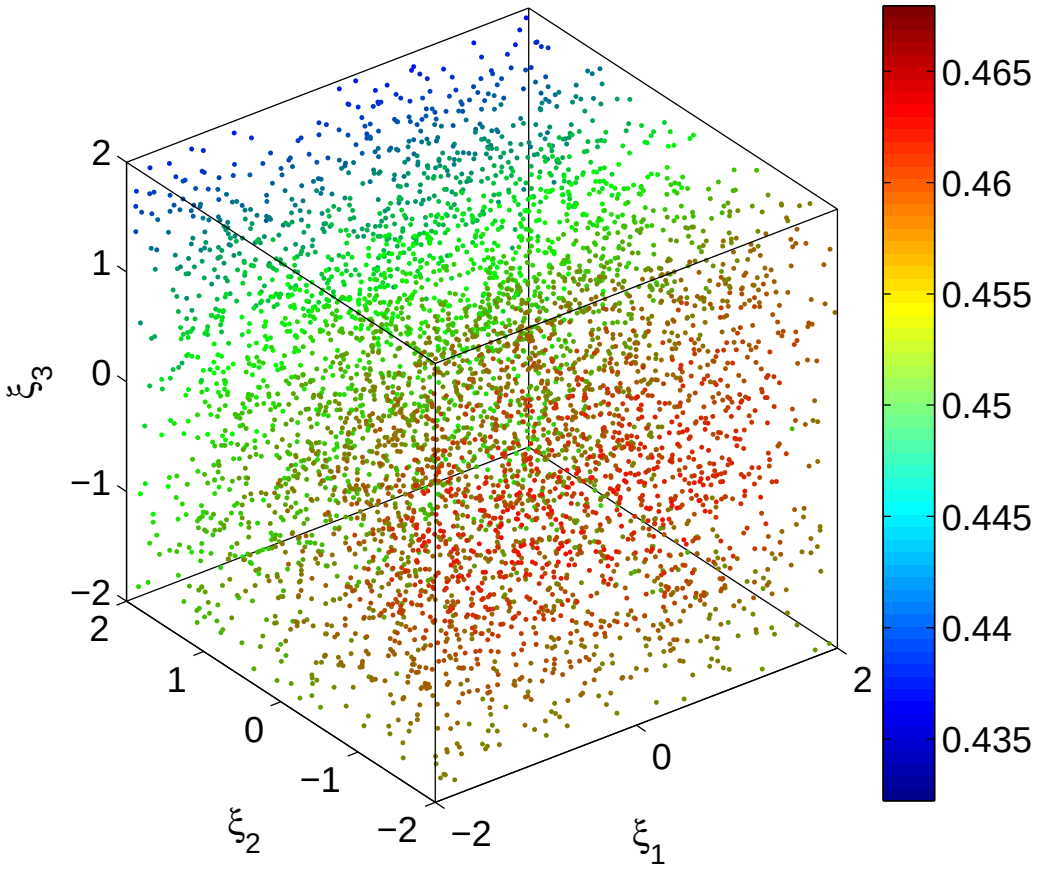

Figure 16. Monte Carlo samples for manufacturing errors

In this framework we observed a reduction of the power coefficient by up to 7% (Figure 17) with negligible change in the perceived noise.

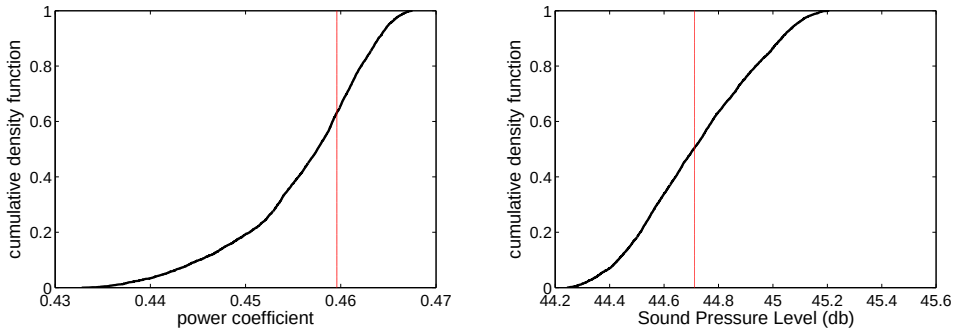

Figure 17. Manufacturing errors: cumulative density function of the power coefficient and Sound Pressure Level

Figure 18 and Figure 19 show the SSC convergence of the mean and standard deviation of the output of interest, revealing that 30 simplex points would have been enough for this analysis.

The mean, standard deviation and coefficient of variation of the analysis under manufacturing errors are

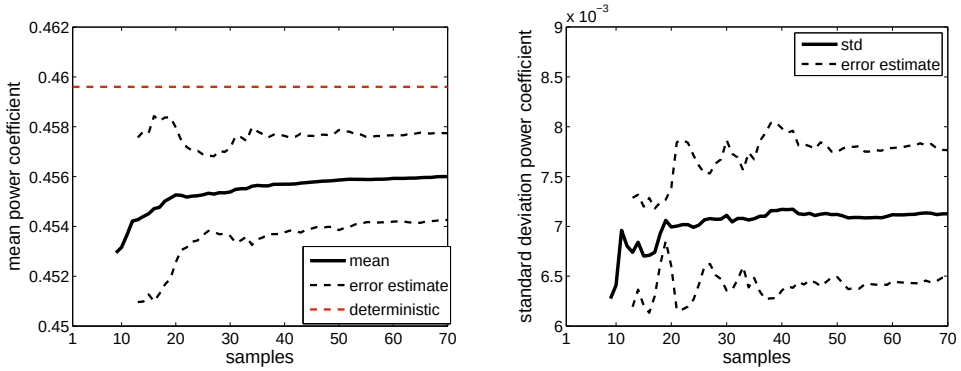

Figure 18. Manufacturing errors: convergence histories of the mean,variance and error of the power coefficient

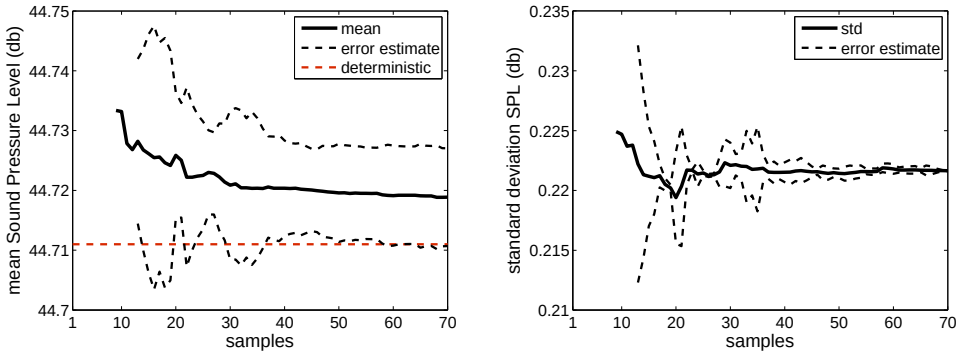

Figure 19. Manufacturing errors: convergence histories of the mean,variance and error of the Sound Pressure Level

summarized in Table 5.

Table 5. Analysis under manufacturing errors

Objective	Mean	Standard deviation	Coefficient of variation	Clean configuration
# Power Coefficient[-]	0.4560	0.0071	0.0156	0.4596
# Sound Pressure Level[*db*]	44.7189	0.2216	0.0050	44.711

The simplex points in probability space for uncertain meteorological conditions, insect contamination and manufacturing errors are represented in Figure 20.

VI. Conclusions

The present study is the first step of a comprehensive analysis of wind turbine performance under uncertainty. We constructed a multi-physics low-order model `EOLO` that includes aerodynamic predictions, comprehensive structural analysis and acoustic estimation. We identified three sources of uncertainty, namely wind condition, insect contamination and manufacturing tolerances, and successfully estimated their effect on aerodynamic performance and noise. Specifically, we demonstrate how the present uncertainties lead to a general decrease in performance with respect to the nominal (design) scenario. This penalization is also compounded with a likely variation in noise. These results indicate that design and optimization steps should include a comprehensive estimation of the uncertainties in order to achieve robust performance. An additional objective of the paper was to compare Latin Hypercube Sampling and Stochastic Simplex Collocation for propagating uncertainties in complex computational models. Both methods outperform classical Monte Carlo and the SSC approach leads to stable statistics requiring only a few dozen `EOLO` simulations.

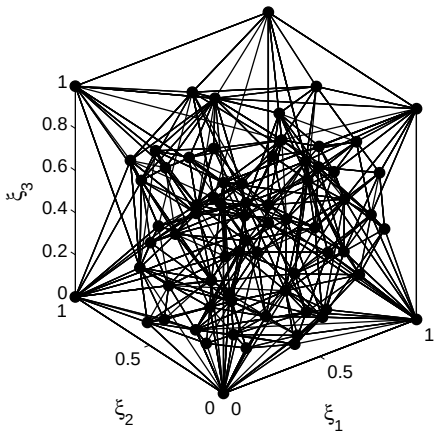

(a) Uncertain metereological conditions

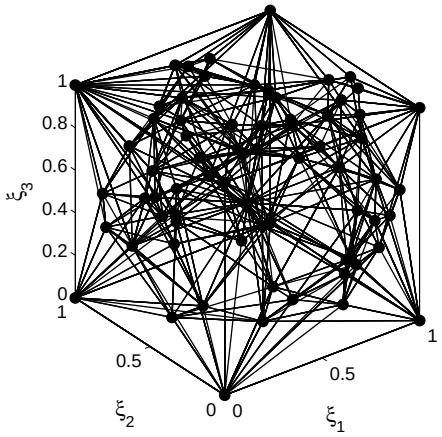

(b) Insect contamination

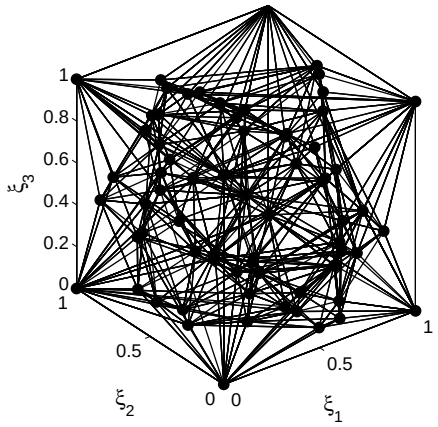

(c) Manufacturing errors

Figure 20. Simplex points in probability space.

Acknowledgments

Support from the Netherlands Organization for Scientific Research (NWO) under the Rubicon Fellowship program is gratefully acknowledged. GP is supported under the exchange program of the XXIV Doctoral Program in Industrial Engineering (Aeronautics) at the Federico II University in Naples, Italy. The authors are also thankful for additional support from the US DOE ASCR program on Uncertainty Quantification (project manager K. Pao).

References

[1]Alonso, J. J., Hahn, S., Ham, F., Herrmann, M., Iaccarino, G., Kalitzin, G., LeGresley, P., Mattsson, K., Medic, G., Moin, P., Pitsch, H., Schluter, J., Svard, M., Van der Weide, E., You, D. and Wu, X., 2006, CHIMPS: A high-performance scalable module for multi physics simulations. AIAA Paper 2006 5274.

[2]NWTC Design Codes (PreComp by Gunjit Bir). http://wind.nrel.gov/designcodes/preprocessors/precomp/. Last modified 26-March-2007; accessed 26-March-2007.

[3]NWTC Design Codes (FAST by Jason Jonkman, Ph.D.). http://wind.nrel.gov/designcodes/simulators/fast/. Last modified 05-November-2010; accessed 05-November-2010.

[4]NWTC Design Codes (AeroDyn by Dr. David J. Laino). http://wind.nrel.gov/designcodes/simulators/aerodyn/. Last modified 31-March-2010; accessed 31-March-2010.

[5]NWTC Design Codes (BModes by Gunjit Bir). http://wind.nrel.gov/designcodes/preprocessors/bmodes/. Last modified 20-March-2008; accessed 20-March-2008.

[6]NWTC Design Codes (TurbSim by Neil Kelley, Bonnie Jonkman). http://wind.nrel.gov/designcodes/preprocessors/turbsim/. Last modified 25-September-2009; accessed 25-September-2009.

[7]Witteveen, J.A.S., Iaccarino, G., Simplex Elements Stochastic Collocation for Uncertainty Propagation in Robust Design Optimization 48th AIAA Aerospace Sciences Meeting, Orlando, Florida (2010) AIAA-2010-1313.

[8]Witteveen, J.A.S., Iaccarino, G., Simplex elements stochastic collocation in higher-dimensional probability spaces, 51st AIAA/ASME/ASCE/AHS/ASC Structures, Structural Dynamics, and Materials Conference, Orlando, Florida (2010) AIAA-2010-2924.

[9]Drela, M., Xfoil: An Analysis and Design System for Low Reynolds Number Airfoils, Low Reynolds Number Aerodynamics (Conference Proceedings), edited by T.J. Mueller, University of Notre Dame 1989.

[10]Tangler, J., Kocurek, J.D., Wind Turbine Post-Stall Airfoil Performance Characteristics Guidelines for Blade-Element Momentum Methods, NREL/CP-500-36900.

[11]Tuller, S.E., Brett, A.C., The characteristics of wind velocity that favor the fitting of a Weibull distribution in wind speed analysis. Journal of Climate and Applied Meteorology, 23:124134, 1984.

[12]Antoniou,I., Petersen,S.M., HÃ¸jstrup,J. et al., Identification of variables for site calibration and power curve assessment in complex terrain. Technical Report JOR3-CT98-0257, RisÃ¸, CRES, WindTest, DEWI, ECN, Bonus and NEG Micon, July 2001.

[13]Lange,B., Modelling the Marine Boundary Layer for Offshore Wind Power Utilisation. PhD thesis, University of Oldenburg, December 2002.

[14]Wieringa,J., Rijkoort,P.J., Windklimaat van Nederland (Wind Climate of the Netherlands). KNMI/Staatsuitgeverij, Den Haag, 1983.

[15]Downey,R.P., Uncertainty in wind turbine life equivalent load due to variation of site conditions. Masters thesis, Technical University of Denmark, Fluid Mechanics Section, Lyngby, April 2006.

[16]Veldkamp, D., Chances in Wind Energy - A probabilistic Approach to Wind Turbine Fatigue Design. PhD thesis, Delft University.

[17]Corten G. , Veldkamp H., Insects cause double stall, EWEC Copenhagen , 2001.

[18]Corten, G.P., Insects Cause Double Stall, ECN-CX–00-018, Feb. 2001

[19]Dyrmose, S.Z., Hansen, P., The Double Stall Phenomenon and how to avoid it , IEA, Lyngby, 1998.

[20]Madsen, H.A., Aerodynamics of a Horizontal Axis Wind Turbine in Natural Conditions, Risoe M 2903 1991.

[21]Iachmann, H.S., Aspects of Insect Contamination in Relation to Laminar Flow Aircraft, Aeronautical Research Council current, April 1959.

[22]Croom, C. C.; and Holmes, B. J.: Flight Evaluation of an Insect Contamination Protection System for Laminar Flow Wings. SAE Paper 850860, April 1985.

[23]Hardy, A. C.; and Milne, P. S.: Studies in the Distribution of Insects by Aerial Currents. Journal of Animal Ecology, vol. 7, 1938, pp. 199-229.

[24]Brooks, T., Pope, D., and Marcolini, M., Airfoil Self-Noise and Prediction, NASA Reference Publication 1218, National Aeronautics and Space Administration, 1989.

[25]Crouch, J.D., Kosorygin, L.L. , Modeling the effects of steps on boundary layer transition, IUTAM Symposium on Laminar-Turbulent Transition, 2006.

[26]Moriarty, P., and Migliore, P., 2003 Semi-empirical aeroacoustic noise prediction code for wind turbines National Renewable Energy Laboratory

[27]Ilinca, F., Hay, A., and Pelletier, D., Shape Sensitivity Analysis of Unsteady Laminar Flow Past a Cylinder in Ground Proximity, Proceedings of the 36th AIAA Fluid Dynamics Conference and Exhibit , AIAA paper 2006 3880, San Francisco, June 2006.

[28]Etienne, S., Hay, A., Garon, A., and Pelletier, D., Shape Sensitivity Analysis of Fluid-Structure Interaction Problems, Proceedings of the 36th AIAA Fluid Dynamics Conference and Exhibit , AIAA paper 2006 3217, San Francisco, June 2006.

[29]Gumber, C. R., Newman, P. A., and Hou, G. J. W., Effect of Random Geometric Uncertainty on the Computational Design of a 3D Flexible Wing, Proceedings of the 20th AIAA Applied Aerodynamics Conference, AIAA paper 2002 2806, St. Louis, June 2002.

[30]Loeven, G.J.A. and Bijl, H., Airfoil Analysis with Uncertain Geometry using the Probabilistic Collocation method, Proc. of the AIAA 48th AIAA/ASME/ASCE/AHS/ASC Structures, Structural Dynamics, and Materials Conference, Schaumburg (IL), United States, 2008.

[31]Iman, R. L. and Conover, W. J. (1980), Small Sample Sensitivity Analysis Techniques for Computer Models, with An Application to Risk Assessment, Communications in Statistics, A9(17), 1749-1842. Rejoinder to Comments, 1863-1874.

[32]Wyss, G.D. and Jorgensen, K.H. (1998) A user's guide to LHS: Sandia's Latin hypercube sampling software. Available online at: http://www.prod.sandia.gov/cgi-bin/techlib/access-control.pl/ 1998/980210.pdf

[33]IEC 61400-1 (1999) Wind turbine generator systems-Part 1: Safety requirements, 2nd edition. International Electrotechnical Commission.

[34]IEC 61400-1 (August 2005) Wind turbines-Part 1: Design requirements, 3rd edition. International Electrotechnical Commission.